

OBLIQUE STAGNATION POINT FLOW OF A NON-NEWTONIAN NANOFLUID OVER STRETCHING SURFACE WITH RADIATION A Numerical Study

by

Abuzar GHAFARI^{a*,}, Tariq JAVED^a, and Fotini LABROPULU^b**

^a Department of Mathematics and Statistic, International Islamic University, Islamabad, Pakistan

^b Department of Mathematics, Luther College, University of Regina, Regina, Canada

Original scientific paper

<https://doi.org/10.2298/TSCI150411163G>

In this study, we discussed the enhancement of thermal conductivity of elastico-viscous fluid filled with nanoparticles, due to the implementation of radiation and convective boundary condition. The flow is considered impinging obliquely in the region of oblique stagnation point on the stretching surface. The obtained governing partial differential equations are transformed into a system of ordinary differential equations by employing a suitable transformation. The solution of the resulting equations is computed numerically using Chebyshev spectral newton iterative scheme. An excellent agreement with the results available in literature is obtained and shown through tables. The effects of involving parameters on the fluid flow and heat transfer are observed and shown through graphs. It is importantly noted that the larger values of Biot number imply the enhancement in heat transfer, thermal boundary layer thickness, and concentration boundary layer thickness.

Key words: *thermal conductivity, elastico-viscous fluid, oblique stagnation point, spectral method*

Introduction

Oblique stagnation-point flow appears when fluid from any source impinges obliquely on a rigid wall at an arbitrary angle of incidence as shown in fig. 1. Many researchers have studied the steady 2-D oblique stagnation-point flow of a Newtonian fluid. Stuart [1] did the pioneer work in this field, later studied by Tamada [2] and Dorrepaal [3]. Recently, Reza and Gupta [4] generalized the problem of Chiam [5] by introducing a stretching surface. In their paper, they ignored the displacement thickness and pressure gradient. This was partially rectified in a paper by Lok *et al.* [6]. Very recently, Reza and Gupta [7] gave a correct solution to the problem by fixing the errors in [4] and [6]. Drazin and Riley [8], Tooke and Blyth [9] reviewed the problem and included a free parameter associated with the shear flow component related to the pressure gradient. Weidman and Putkaradze [10, 11] studied the steady-oblique stagnation-point flow impinging on a circular cylinder. The flow is described using a coupled set of ordinary differential equations. Recently, Erfani *et al.* [12], Husain *et al.* [13], Mahapatra *et al.* [14], Lok *et al.* [15], Yajun and Liancun [16], and Javed *et al.* [17] have done notable work on orthogonal and oblique stagnation point flow.

*Corresponding author, e-mail: abuzar.iiui@gmail.com

**Now in Department of Mathematics, University of Education, Lahore, Pakistan

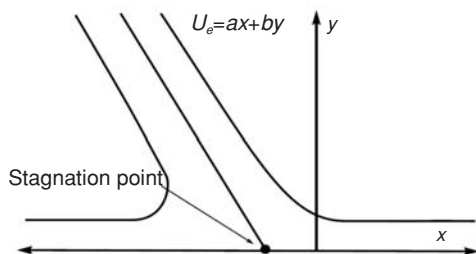


Figure 1. Physical Model

In last few decades, heat transfer in nanofluids has become a topic of major interest. Many researchers contributed in this area due its significance in pharmaceutical and food processes, hyperthermia, fuel cells, micro-electronics, hybrid-powered engines, coolants for advanced nuclear power plants [18] and many others. The basic idea of using nanosized particle to enhance the thermal conductivity of the fluid was given by Maxwell [19]. Choi [20] was the first who introduced the term nanofluid in 1995. He studied the characteristics of nanofluids and deduced that the thermal conductivity of the base fluid (water, oil, biofluids, organic liquids, ethylene glycol, etc.) can be enhanced by introducing metallic particles (average size about 10 nanometers). Nanoparticles are made of different metals (Al, Cu, Ag, Au, Fe), metal carbides (SiC) non-metals (graphite carbon nanotubes), oxides (Al_2O_3 , CuO, TiO_2), nitrides (AlN, SiN), etc. In 2006, Buongiorno [21] has studied the convective transport in fluid and he considered seven slip mechanisms (thermophoresis, diffusiophoresis, Brownian diffusion, inertia, Magnus effect, gravity, and fluid drainage) to discuss the relative velocity of the fluid and nanoparticles and he concluded that among these seven slip mechanisms only two are important. Recently, Kuznetsov and Nield [22, 23] studied the double-diffusive and natural convective boundary-layer flow of a nanofluid past a vertical plate, they found the analytical solution of the problems. Makinde and Aziz [24] studied the convective heat transfer in nanofluid past a stretching sheet and they discussed Brownian motion and thermophoresis effects in detail. There is extensive literature available on the topic through different aspects. Few representative recent studies on the topic may be seen in the refs. [25-38].

Literature survey witnessed that much attention in the past has been accorded to the flow of viscous nanofluids. However, in real situation the base fluids in the nanomaterials is not viscous. No doubt, the base fluid in reality is viscoelastic. Mention may be made to some viscoelastic nanofluids like ethylene glycol-CuO, ethylene glycol- Al_2O_3 , ethylene glycol-ZnO. Keeping such preference in view the viscoelastic nanofluid is considered in this paper. Many viscoelastic fluids models have been proposed but here constitutive equations of Walter-B fluid [39-41] are employed in the mathematical formulation. Our intention here is to compute the oblique stagnation point flow of viscoelastic nanofluid. To the best of our knowledge, such problem has not been attempted before. An efficient approach namely the Chebyshev Spectral Newton Iterative Scheme (CSNIS) is implemented for the numerical solution. The graphical results are interpreted with respect to various parameters of interest. A comparison with the previously published results in limiting sense is given. Heat transfer rate and mass diffusion flux are also analyzed.

Problem formulation

We consider the steady 2-D laminar flow of Walter-B nanofluid impinging obliquely on a stretching surface, which is placed at $\bar{y} = 0$ and the fluid occupies the upper half plane $\bar{y} > 0$ as shown in fig. 1. The surface is heated convectively, by convective heating process, which is characterized by a temperature, T_f , and a heat transfer coefficient, h_f . We neglect the viscous dissipation to estimate accurately the effect of convective boundary condition because viscous dissipation would disturb the thermal boundary conditions. The velocity of the outer flow far away from the surface is $U_e(\bar{x}, \bar{y}) = a\bar{x} + b\bar{y}$. The flow, energy and concentration equations are, see Beard and Walters [41].

$$\frac{\partial \bar{u}}{\partial \bar{x}} + \frac{\partial \bar{v}}{\partial \bar{y}} = 0 \quad (1)$$

$$\begin{aligned} \bar{u} \frac{\partial \bar{u}}{\partial \bar{x}} + \bar{v} \frac{\partial \bar{u}}{\partial \bar{y}} = & -\frac{1}{\rho} \frac{\partial \bar{p}}{\partial \bar{x}} + \nu \left(\frac{\partial^2 \bar{u}}{\partial \bar{x}^2} + \frac{\partial^2 \bar{u}}{\partial \bar{y}^2} \right) + \frac{k_o}{\rho} \left\{ \frac{\partial}{\partial \bar{x}} \left[2\bar{u} \frac{\partial^2 \bar{u}}{\partial \bar{x}^2} + 2\bar{v} \frac{\partial^2 \bar{u}}{\partial \bar{x} \partial \bar{y}} + 4 \left(\frac{\partial \bar{u}}{\partial \bar{x}} \right)^2 + 2 \frac{\partial \bar{v}}{\partial \bar{x}} \left(\frac{\partial \bar{v}}{\partial \bar{x}} + \frac{\partial \bar{u}}{\partial \bar{y}} \right) \right] \right. \\ & \left. + \frac{\partial}{\partial \bar{y}} \left[\left(\bar{u} \frac{\partial}{\partial \bar{x}} + \bar{v} \frac{\partial}{\partial \bar{y}} \right) \left(\frac{\partial \bar{v}}{\partial \bar{x}} + \frac{\partial \bar{u}}{\partial \bar{y}} \right) + 2 \frac{\partial \bar{u}}{\partial \bar{x}} \frac{\partial \bar{u}}{\partial \bar{y}} + 2 \frac{\partial \bar{v}}{\partial \bar{x}} \frac{\partial \bar{v}}{\partial \bar{y}} \right] \right\} \end{aligned} \quad (2)$$

$$\begin{aligned} \bar{u} \frac{\partial \bar{v}}{\partial \bar{x}} + \bar{v} \frac{\partial \bar{v}}{\partial \bar{y}} = & -\frac{1}{\rho} \frac{\partial \bar{p}}{\partial \bar{y}} + \nu \left(\frac{\partial^2 \bar{v}}{\partial \bar{x}^2} + \frac{\partial^2 \bar{v}}{\partial \bar{y}^2} \right) + \frac{k_o}{\rho} \left\{ \frac{\partial}{\partial \bar{x}} \left[2 \frac{\partial \bar{u}}{\partial \bar{x}} \frac{\partial \bar{u}}{\partial \bar{y}} + 2 \frac{\partial \bar{v}}{\partial \bar{x}} \frac{\partial \bar{v}}{\partial \bar{y}} + \left(\bar{u} \frac{\partial}{\partial \bar{x}} + \bar{v} \frac{\partial}{\partial \bar{y}} \right) \left(\frac{\partial \bar{v}}{\partial \bar{x}} + \frac{\partial \bar{u}}{\partial \bar{y}} \right) \right] \right. \\ & \left. + \frac{\partial}{\partial \bar{y}} \left[2 \frac{\partial \bar{u}}{\partial \bar{y}} \left(\frac{\partial \bar{v}}{\partial \bar{x}} + \frac{\partial \bar{u}}{\partial \bar{y}} \right) + 4 \left(\frac{\partial \bar{v}}{\partial \bar{y}} \right)^2 + 2\bar{v} \frac{\partial^2 \bar{v}}{\partial \bar{y}^2} + 2\bar{u} \frac{\partial^2 \bar{v}}{\partial \bar{x} \partial \bar{y}} \right] \right\} \end{aligned} \quad (3)$$

$$\bar{u} \frac{\partial \bar{T}}{\partial \bar{x}} + \bar{v} \frac{\partial \bar{T}}{\partial \bar{y}} = \frac{k}{\rho C_p} \left(\frac{\partial^2 \bar{T}}{\partial \bar{x}^2} + \frac{\partial^2 \bar{T}}{\partial \bar{y}^2} \right) - \frac{1}{\rho C_p} \frac{\partial q_r}{\partial \bar{y}} + \tau \left\{ D_B \left(\frac{\partial \bar{C}}{\partial \bar{x}} \frac{\partial \bar{T}}{\partial \bar{x}} + \frac{\partial \bar{C}}{\partial \bar{y}} \frac{\partial \bar{T}}{\partial \bar{y}} \right) + \frac{D_T}{T_\infty} \left[\left(\frac{\partial \bar{T}}{\partial \bar{x}} \right)^2 + \left(\frac{\partial \bar{T}}{\partial \bar{y}} \right)^2 \right] \right\} \quad (4)$$

$$\bar{u} \frac{\partial \bar{C}}{\partial \bar{x}} + \bar{v} \frac{\partial \bar{C}}{\partial \bar{y}} = D_B \left(\frac{\partial^2 \bar{C}}{\partial \bar{x}^2} + \frac{\partial^2 \bar{C}}{\partial \bar{y}^2} \right) + \frac{D_T}{T_\infty} \left(\frac{\partial^2 \bar{T}}{\partial \bar{x}^2} + \frac{\partial^2 \bar{T}}{\partial \bar{y}^2} \right) \quad (5)$$

In previous equations, $\bar{u}(\bar{x}, \bar{y})$ and $\bar{v}(\bar{x}, \bar{y})$ are the velocity components in \bar{x} - and \bar{y} -directions, $\bar{C}(\bar{x}, \bar{y})$ – the concentration, $\bar{T}(\bar{x}, \bar{y})$ – the temperature, and $\bar{p}(\bar{x}, \bar{y})$ – the pressure of the fluid flow. Also, ν – the kinematic viscosity, ρ – the density, k_o – the elasticity of fluid, C_p – the specific heat, k – the thermal conductivity of the fluid, and q_r – the radiative heat flux. The D_T and D_B are the Brownian motion coefficient and thermophoretic diffusion coefficient, respectively, and $\tau = (\rho C)_p / (\rho C)_f$ is the ratio of effective heat capacity of nanoparticles materials to heat capacity of the fluid. The boundary conditions of the problem can be defined:

$$\bar{y} = 0: \bar{u} = c\bar{x}, \bar{v} = 0, \quad -k \frac{\partial \bar{T}}{\partial \bar{y}} = h_f (T_f - \bar{T}), \quad \bar{C} = C_w \quad (6)$$

$$\bar{y} \rightarrow \infty: \bar{u} = a\bar{x} + b\bar{y}, \quad \bar{T} = T_\infty, \quad \bar{C} = C_\infty$$

in which a , b , and c are positive constants having the dimension of inverse time, T_∞ – the ambient temperature, and h_f – the heat transfer coefficient. The radiative heat flux can be modeled by using Rosseland's approximation:

$$q_r = -\frac{4\sigma}{3(\alpha_r + \sigma_s)} \frac{\partial \bar{T}^4}{\partial \bar{y}} \quad (7)$$

where σ is the Stefan-Boltzmann constant, α_r – the Rosseland mean absorption coefficient, and σ_s – the scattering coefficient. Assuming that the temperature difference within the flow is sufficient small so that \bar{T}^4 may be expressed as linear function T such that:

$$\bar{T}^4 = 4T_\infty^3 \bar{T} - 3T_\infty^4 \quad (8)$$

thus eq. (7) takes the following form:

$$q_r = -\frac{16\sigma T_\infty^3}{3(\alpha_r + \sigma_s)} \frac{\partial \bar{T}}{\partial \bar{y}} \quad (9)$$

Upon using non-dimensional variables and stream function, ψ , this satisfies the continuity equation such:

$$x = \bar{x} \sqrt{\frac{c}{\nu}}, \quad y = \bar{y} \sqrt{\frac{c}{\nu}}, \quad u = \frac{1}{\sqrt{\nu c}} \bar{u}, \quad v = \frac{1}{\sqrt{\nu c}} \bar{v}, \quad p = \frac{1}{\rho \nu c} \bar{p}, \quad T = \frac{\bar{T} - T_\infty}{T_f - T_\infty}, \quad C = \frac{\bar{C} - C_\infty}{C_w - C_\infty}, \quad (10)$$

$$u = \frac{\partial \psi}{\partial y}, \quad v = -\frac{\partial \psi}{\partial x}$$

and then eliminating pressure from eqs. (2) and (3), eqs. (2)-(6) take the following new form in term of ψ :

$$\frac{\partial(\psi, \nabla^2 \psi)}{\partial(x, y)} + \text{We} \frac{\partial(\psi, \nabla^4 \psi)}{\partial(x, y)} + \nabla^4 \psi = 0 \quad (11)$$

$$\frac{\partial \psi}{\partial y} \frac{\partial T}{\partial x} - \frac{\partial \psi}{\partial x} \frac{\partial T}{\partial y} = \frac{1}{\text{Pr}} \left(\frac{\partial^2 T}{\partial x^2} + \frac{\partial^2 T}{\partial y^2} + \frac{16\sigma T_\infty^3}{3k(\alpha_r + \sigma_s)} \frac{\partial^2 T}{\partial y^2} \right) + N_b \left(\frac{\partial C}{\partial x} \frac{\partial T}{\partial x} + \frac{\partial C}{\partial y} \frac{\partial T}{\partial y} \right) + N_t \left[\left(\frac{\partial T}{\partial x} \right)^2 + \left(\frac{\partial T}{\partial y} \right)^2 \right] \quad (12)$$

$$\text{Sc} \left(\frac{\partial \psi}{\partial y} \frac{\partial C}{\partial x} - \frac{\partial \psi}{\partial x} \frac{\partial C}{\partial y} \right) = \left(\frac{\partial^2 C}{\partial x^2} + \frac{\partial^2 C}{\partial y^2} \right) + \frac{N_t}{N_b} \left(\frac{\partial^2 T}{\partial x^2} + \frac{\partial^2 T}{\partial y^2} \right) \quad (13)$$

$$y = 0: \quad \frac{\partial \psi}{\partial y} = x, \quad \psi = 0, \quad \frac{\partial T}{\partial y} = -\text{Bi}(1 - T), \quad C = 1$$

$$y \rightarrow \infty: \quad \psi = \frac{a}{c} xy + \frac{\gamma}{2} y^2, \quad T = 0_\infty, \quad C = 0 \quad (14)$$

where $\text{We} = k_0 c / \rho \nu$ is the Weissenberg number, $\text{Pr} = \mu C_p / k$ – the Prandtl number, $\text{Sc} = \nu / D_B$ – the Schmidt number, $N_t = D_T \tau (T_f - T_\infty) / T_\infty \nu$ – the thermophoresis parameter, $N_b = D_B \tau (C_w - C_\infty) / \nu$ – the Brownian motion parameter, $\text{Bi} = -(h_f / k)(\nu / c)^{1/2}$ – the Biot number, and $\gamma = b / c$ represents shear in the free stream. Suppose the solution of eqs. (11-14) is of the form:

$$\psi = xf(y) + g(y), \quad T = \theta(y), \quad C = \phi(y) \quad (15)$$

where the functions $f(y)$ and $g(y)$ are normal and oblique component of the flows. Using the eq. (15) in eqs. (11)-(14), and after comparing the coefficient of x^0 and x^1 , we get:

$$f^{iv} + ff''' - f'f'' + \text{We}(ff'v - f'f^{iv}) = 0 \quad (16)$$

$$g^{iv} + fg''' - g'f'' + \text{We}(fg'v - g'f^{iv}) = 0 \quad (17)$$

$$\left(1 + \frac{4}{3} Rd \right) \theta'' + \text{Pr} \left[f\theta' + N_b \phi' \theta' + N_t (\theta')^2 \right] = 0 \quad (18)$$

$$\phi'' + \text{Sc} f \phi' + \frac{N_t}{N_b} \theta'' = 0 \quad (19)$$

$$\begin{aligned} y=0: \quad f(y)=0, \quad f'(y)=1, \quad g(y)=g'(y)=0, \quad \theta'(y)=-\text{Bi}[1-\theta(y)], \quad \phi(y)=1 \\ y \rightarrow \infty: \quad f'(y)=a/c, \quad g'(y)=\gamma y, \quad \theta(y)=0, \quad \phi(y)=0 \end{aligned} \quad (20)$$

where $Rd = 4\sigma T_\infty^3 / k(\alpha_r + \sigma_s)$ is the radiation parameter and prime denotes the differentiation with respect to y . After integrating eqs. (16) and (17) the resulting constants of integration can be evaluated by employing the boundary conditions at infinity and we get:

$$f''' + ff'' - (f')^2 + \text{We} \left[f^{iv} - 2f'f''' + (f'')^2 \right] + \frac{a^2}{c^2} = 0 \quad (21)$$

$$g''' + fg'' - g'f' + \text{We} \left(fg^{iv} - f'g''' + g''f'' - f'''g' \right) - A\gamma = 0 \quad (22)$$

where $A = A(a/c, \text{We})$ is a constant which measures the boundary layer displacement. Constant A at free stream behave as $(a/c)y$ which also corresponds to the behavior of $f(y)$ at the free stream. For simplicity, introducing a new variable, $g'(y) = \gamma h(y)$, then eq. (22) with boundary conditions is written:

$$h'' + fh' - f'h + \text{We} \left(fh''' - f'h'' + h'f'' - f'''h \right) = A \quad (23)$$

$$h(0)=0 \quad h'(\infty)=1 \quad (24)$$

Thus the system of non-linear ordinary equations becomes:

$$f''' + ff'' - (f')^2 + \text{We} \left[ff^{iv} - 2f'f''' + (f'')^2 \right] + \frac{a^2}{c^2} = 0 \quad (25)$$

$$h'' + fh' - f'h + \text{We} \left(fh''' - f'h'' + h'f'' - f'''h \right) = A \quad (26)$$

$$\left(1 + \frac{4}{3} Rd \right) \theta'' + \text{Pr} \left[f\theta' + N_b \phi' \theta' + N_t (\theta')^2 \right] = 0 \quad (27)$$

$$\phi'' + \text{Sc} f \phi' + \frac{N_t}{N_b} \theta'' = 0 \quad (28)$$

with boundary conditions

$$\begin{aligned} y=0: \quad f(y)=0, \quad f'(y)=1, \quad h(y)=0, \quad \theta'(y)=-\text{Bi}[1-\theta(y)], \quad \phi(y)=1 \\ y \rightarrow \infty: \quad f'(y)=a/c, \quad h'(y)=1, \quad \theta(y)=0, \quad \phi(y)=0 \end{aligned} \quad (29)$$

To solve the fourth order ordinary differential eqs. (25) and (26), we used two extra boundary conditions $f''(y)=0$ and $h''(y)=0$ as $y \rightarrow \infty$. These conditions are called augmented boundary conditions [42, 43]. The dimensionless components of velocity are:

$$u = \frac{\partial \psi}{\partial y} = xf'(y) + g'(y), \quad v = -\frac{\partial \psi}{\partial x} = -f(y) \quad (30)$$

The quantities of physical interest are the skin friction coefficients, C_f , the local Nusselt number, Nu_x , and the local Sherwood number, Sh_x , can be expressed:

$$C_f = \frac{\tau_w}{\rho u_w^2}, \quad Nu_x = \frac{\bar{x}(q_w + q_r)}{k(T_f - T_\infty)}, \quad Sh_x = \frac{\bar{x}q_m}{D_B(C_w - C_\infty)} \quad (31)$$

where τ_w is shear stress at the wall, q_r – the radiative heat flux, q_w and q_m represents local heat flux, and local mass diffusion flux, respectively, at the wall are:

$$\tau_w = \mu(\bar{u}_y + \bar{v}_x) - 2k_0 \left[-\bar{u}_y \bar{v}_y - \bar{u}_x \bar{v}_x - \frac{1}{2} \bar{v}_y (\bar{u}_y + \bar{v}_x) - \frac{1}{2} \bar{u}_x (\bar{u}_y + \bar{v}_x) + \frac{1}{2} \bar{v} (\bar{u}_{yy} + \bar{v}_{yy}) + \frac{1}{2} \bar{u} (\bar{u}_{xy} + \bar{v}_{xx}) \right] \Big|_{y=0} \quad (32)$$

$$q_w = -k \left(\frac{\partial \bar{T}}{\partial y} \right) \Big|_{y=0}, \quad q_m = -D_B \left(\frac{\partial \bar{C}}{\partial y} \right) \Big|_{y=0}, \quad q_r = -\frac{4\sigma}{3(\alpha_r + \sigma_s)} \frac{\partial \bar{T}^4}{\partial y}$$

After using eqs. (10) and (15), the skin friction coefficients, C_f , the local Nusselt number, Nu_x , and the local Sherwood number, Sh_x , takes the following form:

$$Re_x C_f = x(1 - 3We)f''(0) + (1 - 2We)\gamma h'(0)$$

$$Re_x^{-1/2} Nu_x = -\left(1 + \frac{4}{3} Rd\right) \theta'(0), \quad Re_x^{-1/2} Sh_x = -\phi'(0) \quad (33)$$

where $Re_x = u_w x / \nu$.

Numerical method

Exact solutions of the non-linear differential eqs. (25)-(28) subject to the boundary conditions (29) are very rare due to the non-linearity. Some authors have used analytical semi-analytical techniques to solve these eqs. (33) and (39). In the present study, we used a numerical technique named as CSNIS. In this scheme, we first convert the system of non-linear differential equation into a linear form by using Newton iterative scheme. For $(i+1)^{th}$ iterates, we write:

$$f_{i+1} = f_i + \delta f_i, \quad \theta_{i+1} = \theta_i + \delta \theta_i, \quad \phi_{i+1} = \phi_i + \delta \phi_i, \quad (34)$$

for all dependent variables, where δf_i , $\delta \theta_i$ and $\delta \phi_i$, represents a very small change in f_i , θ_i , and ϕ_i respectively. The equations (25)-(28) in linearized form are:

$$a_{0,i} \delta f_i^{iv} + a_{1,i} \delta f_i''' + a_{2,i} \delta f_i'' + a_{3,i} \delta f_i' + a_{4,i} \delta f_i = R_{1,i}$$

$$b_{0,i} \delta f_i''' + b_{1,i} \delta f_i'' + b_{2,i} \delta f_i' + b_{3,i} \delta f + b_{4,i} \delta h_i''' + b_{5,i} \delta h_i'' + b_{6,i} \delta h_i' + b_{7,i} \delta h_i = R_{2,i} \quad (35)$$

$$c_{0,i} \delta f + c_{1,i} \delta \theta_i' + c_{2,i} \delta \theta_i + c_{3,i} \delta \phi_i' = R_{3,i}$$

$$d_{0,i} \delta f + d_{1,i} \delta \theta_i'' + d_{2,i} \delta \phi_i'' + d_{3,i} \delta \phi_i' = R_{4,i}$$

subject to boundary conditions

$$\delta f_i(0) = -f_i(0), \quad \delta f_i'(0) = a/c - f_i'(0), \quad \delta f_i'(\infty) = 1 - f_i'(\infty), \quad \delta f_i''(\infty) = -f_i''(\infty)$$

$$\delta h_i(0) = -h_i(0), \quad \delta h_i'(\infty) = 1 - h_i'(\infty), \quad \delta h_i''(\infty) = -h_i''(\infty) \quad (36)$$

$$\delta \theta_i'(0) - Bi \delta \theta_i(0) = -\theta_i'(0) - Bi[1 - \theta_i(0)], \quad \delta \theta_i(\infty) = -\theta_i(\infty)$$

The system of linear eq. (35) subject to boundary conditions (36) is solved using the Chebyshev spectral collocation method [44, 45]. For this purpose, the physical domain $[0, \infty]$ is truncated to finite domain $[0, L]$, where L is chosen sufficiently large. The reduced domain is transformed to $[-1, 1]$ by using transformation $\zeta = 2\eta/L - 1$. Nodes from -1 to 1 are defined as $\zeta_j = \cos(\pi j/N)$, $j = 0, 1, 2, \dots, N$, which are known as Gauss-Lobatto collocation points. The Chebyshev spectral collocation method is based on differentiation matrix $[D]$, which can be computed in different ways. Here we used $[D]$ as suggested by Trefethen [46].

The coefficients $a_{j,i}$, $b_{j,i}$, $c_{j,i}$, $d_{j,i}$, and $R_{j,i}$ ($j = 0, 1, 2, 3, \dots$) are

$$\begin{aligned} a_{0,i} &= \text{We } f_i', a_{1,i} = 1 - 2\text{We } f_i', a_{2,i} = f_i - 2\text{We } f_i'', a_{3,i} = -2f_i' - 2\text{We } f_i''', a_{4,i} = f_i'' + \text{We } f_i^{iv} \\ b_{0,i} &= -\text{We } h_i', b_{1,i} = \text{We } h_i'', b_{2,i} = -h_i - \text{We } h_i''', b_{3,i} = h_i' + \text{We } h_i''', b_{4,i} = \text{We } f_i', b_{5,i} = 1 - \text{We } f_i' \\ b_{6,i} &= f_i + \text{We } f_i'', b_{7,i} = -f_i' - \text{We } f_i''', c_{0,i} = \text{Pr } \theta_i', c_{1,i} = \left(1 + \frac{4}{3}Rd\right), c_{3,i} = \text{Pr}(N_b \theta_i') \\ c_{2,i} &= \text{Pr}\left(f_i + N_b \phi_i' + 2N_t \theta_i'\right), d_{0,i} = \text{Sc } \phi_i', d_{1,i} = (N_t/N_b), d_{2,i} = 1, d_{3,i} = \text{Sc } f_i \\ R_{1,i} &= -\text{We} \left[f_i f_i^{iv} - 2f_i' f_i''' + (f_i')^2 \right] - f_i''' - f_i f_i'' + (f_i')^2 - a^2/c^2 \\ R_{2,i} &= -\text{We} \left(f_i h_i''' - f_i' h_i'' + f_i'' h_i' - f_i''' h_i \right) - h_i'' - f_i h_i' + f_i' h_i + A \\ R_{3,i} &= -\left(1 + \frac{4}{3}Rd\right) \theta_i'' - \text{Pr} \left[f_i \theta_i' + N_b \phi_i' \theta_i' + N_t (\theta_i')^2 \right] \\ R_{4,i} &= -\phi_i'' - \text{Sc } f_i \phi_i' - \frac{N_t}{N_b} \theta_i'' \end{aligned} \quad (37)$$

Applying collocation method to eqs. (35) and (36), the following matrix is obtained:

$$\begin{bmatrix} A_{11} & A_{12} & A_{13} & A_{14} \\ A_{21} & A_{22} & A_{23} & A_{24} \\ A_{31} & A_{32} & A_{33} & A_{34} \\ A_{41} & A_{42} & A_{43} & A_{44} \end{bmatrix} \begin{bmatrix} \delta f_i \\ \delta h_i \\ \delta \theta_i \\ \delta \phi_i \end{bmatrix} = \begin{bmatrix} R_{1,i} \\ R_{2,i} \\ R_{3,i} \\ R_{4,i} \end{bmatrix} \quad (38)$$

where

$$\begin{aligned} A_{11} &= a_{0,i} D^4 + a_{1,i} D^3 + a_{2,i} D^2 + a_{3,i} D + a_{4,i} I, & A_{12} &= 0, & A_{13} &= 0, & A_{14} &= 0 \\ A_{21} &= b_{0,i} D^3 + b_{1,i} D^2 + b_{2,i} D + b_{3,i} I, & A_{22} &= b_{4,i} D^3 + b_{5,i} D^2 + b_{6,i} D + b_{7,i} I, & A_{23} &= 0, & A_{24} &= 0 \\ A_{31} &= c_{0,i} I, & A_{32} &= 0, & A_{33} &= c_{1,i} D^2 + c_{2,i} D, & A_{34} &= c_{3,i} D \\ A_{41} &= d_{0,i} I, & A_{42} &= 0, & A_{43} &= d_{1,i} D^2, & A_{44} &= d_{2,i} D^2 + d_{3,i} D \end{aligned} \quad (39)$$

where I is the identity matrix, $a_{j,i}$, $b_{j,i}$, $c_{j,i}$, $d_{j,i}$, and $R_{j,i}$ ($j = 0, 1, 2, 3, \dots$) are given in eq. (37).

Results and discussion

The non-linear differential eqs. (25)-(28) subject to the boundary conditions (29) are solved numerically for the different values of dimensionless parameters namely Weissenberg number, velocities ratio parameter, a/c , radiation, Rd , thermophoresis, N_t , Brownian motion, N_b , Prandtl number, Schmidt number, and Biot number (tabs. 1-4). The values of $f''(0)$, $-\theta'(0)$ and $-\phi'(0)$ shown in limiting case through tabs. 1 and 2 and numerical values of A , eqs. (38) and (39), in tab. 3. It is found that the results are in excellent agreement with previous investigations published in the literature. The results in term of velocity profile, temperature profile,

Table 1. Comparison of $-\theta'(0)$ for the various values of a/c and Prandtl number in the absence thermophoresis effects and Brownian motion of nanoparticles when $We = 0$, $Rd = 0$, and $Bi \rightarrow \infty$

a/c	Present work	[47]	Present work	[47]	Present work	[47]
	Pr = 1		Pr = 10		Pr = 20	
0.1	0.60215	0.60281	2.31693	2.31684	3.36196	3.36172
0.3	0.64728	0.64732	2.34841	2.34841	3.39149	3.39148
0.8	0.75710	0.75709	2.46778	2.46778	3.51054	3.51054
1.0	0.79788	0.79788	2.52313	2.52313	3.56825	3.56825
2.0	0.97873	0.97872	2.81389	2.81389	3.88689	3.88689
3.0	1.13209	1.13209	3.09751	3.09751	4.21307	4.21307
4.0	1.26733	1.26733	3.36440	3.36441	4.52808	4.52810

Table 3. Numerical values of A for various values of We and a/c

a/c	We			
	0	0.05	0.1	0.2
0.0	1.0000	0.9747	0.9487	0.8944
0.1	0.7917	0.7663	0.7402	0.6854
0.2	0.6407	0.6161	0.5906	0.5369
0.3	0.5195	0.4962	0.4720	0.4205
0.4	0.4173	0.3959	0.3735	0.3254
0.5	0.3286	0.3096	0.2896	0.2459
0.6	0.2499	0.2338	0.2167	0.1789
0.7	0.1791	0.1664	0.1527	0.1220
0.8	0.1145	0.1056	0.0960	0.0738
0.9	0.0551	0.0505	0.0454	0.0334
1.0	0.0000	0.0000	0.0000	0.0000

Table 2. Comparison of $-\theta'(0)$ and $-\phi'(0)$ for the various values of N_t and N_b when $We = 0$, $a/c = 0$, $Rd = 0$, $Pr = 10$, $Sc = 10$, and $Bi = 0.1$

N_t	$N_b = 0.1$	
	$-\theta'(0)$	$-\phi'(0)$
0.1	(0.0929) 0.09291	(2.2774) 2.27741
0.3	(0.0925) 0.09255	(2.2228) 2.22281
0.5	(0.0921) 0.09212	(2.1783) 2.17834
N_t	$N_b = 0.3$	
	$-\theta'(0)$	$-\phi'(0)$
0.1	(0.0769) 0.07688	(2.3299) 2.32994
0.3	(0.0729) 0.07292	(2.3900) 2.38996
0.5	(0.0700) 0.06697	(2.4792) 2.47923
N_t	$N_b = 0.5$	
	$-\theta'(0)$	$-\phi'(0)$
0.1	(0.0383) 0.03833	(2.3560) 2.35603
0.3	(0.0269) 0.02690	(2.4576) 2.45762
0.5	(0.0180) 0.01800	(2.5435) 2.54352

The results in small brackets are reported by Makinde and Aziz [24]

Table 4. Numerical values of $Re_x^{-1/2} Nu_x$ and for wider range of Pr

We	a/c	Rd	N_t	N_b	Bi	Sc	Pr	$Re_x^{-1/2} Nu_x$	$Re_x^{-1/2} Sh_x$
0.10	0.10	1	0.1	0.1	0.1	1	0.7	0.1681	0.5539
							1	0.1786	0.5489
							10	0.2164	0.5225
							50	0.2250	0.5107
							100	0.2268	0.5075
0.20	0.50	2	0.3	0.3	1	5	0.7	0.7404	1.5984
							1	0.8434	1.5899
							10	1.3282	1.5803
							50	0.4836	1.9263
							100	0.0776	2.0450
0.3	1.0	5	0.5	0.5	∞	10	0.7	1.7315	2.5104
							1	2.0139	2.5078
							10	3.0888	2.6083
							50	0.5032	2.9136
							100	-0.0194	2.9281

concentration profile, $f''(0)$, $-\theta'(0)$ and $-\phi'(0)$ for sundry parameters are shown through graphs. In most cases, the values of the parameters are taken as $Pr = 6.8$, $Sc = 1.5$, $Bi = 0.5$, $We = 0.1$, $N_t = N_b = 0.3$, $a/c = 0.3, 1.2$, and $Rd = 1$ or otherwise mentioned.

The variation of $f''(0)$, $-\theta'(0)$ and $-\phi'(0)$ against Weissenberg number for $a/c = 0.8, 1.0, 1.1$, and 1.2 are shown in figs. 2-4, respectively. From these figures, it is observed that the similarity eqs. (25)-(28) subject to the boundary conditions (29) have dual solutions in some range of the parameter Weissenberg number. There exist unique solution in particular range of the parameter Weissenberg number and there exist a region where the solution of the equation does not exist. The solid lines show the stable solution and dashed lines show the unstable solution. For $a/c > 1$, the range of solution enhances due to increase in a/c and for $a/c < 1$ the range of unstable solution become larger than the stable solution.

There exist a unique solution at critical value $We = We_c$, dual solution exist between the range $0 \leq We < We_c$ and no solution exists for $We < 0$ and $We > We_c$. The critical values are $We_{c1} = 0.3149$, $We_{c2} = 0.3642$, $We_{c3} = 0.528$, and $We_{c4} = 0.33$ for different values of a/c as shown in figures. It is observed that unstable solution has higher values of $f''(0)$, $-\theta'(0)$, and $-\phi'(0)$ than that of the stable solution for given values of Weissenberg number. It is further noted that in stable solution (first solution) heat and mass transfer rate increase with increase in the values of a/c , where a reverse behavior has been observed for unstable solution (second solution).

The stability analysis of multiple solutions has been discussed by many researcher [48-50]. They found that first solution is applicable physically while the second solution is not. In fig. 5 the velocity profile is plotted against y for the different values of Weissenberg number, a/c , and γ . Here $\gamma = 0$ and $\gamma = 0.2$ correspond to the case for orthogonal stagnation point flow and non-orthogonal stagnation point flow, respectively. It is noted that the velocity of the fluid is increasing with increase in the values of We when $a/c > 1$. An opposite behavior is observed for the case when $a/c < 1$.

It is also seen that with increase in the values of γ the velocity of the fluid increases. In figs. 6 and 7 the variation of local Nusselt, $Re_x^{-1/2}Nu_x$, and local

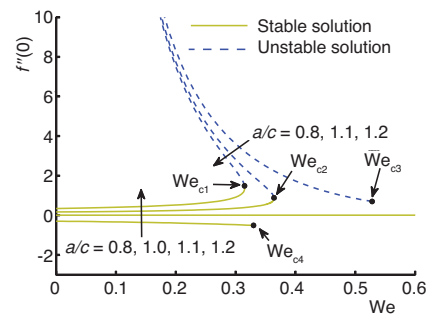


Figure 2. Variation of $f''(0)$ against We for the different values of a/c

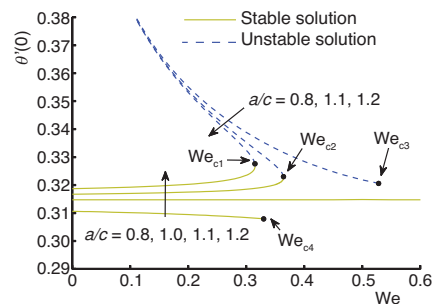


Figure 3. Variation of $-\theta'(0)$ against We for the different values of a/c

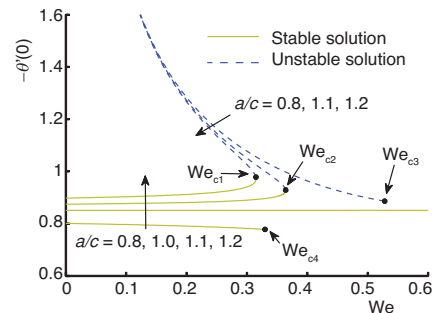


Figure 4. Variation of $-\phi'(0)$ against We for the different values of a/c

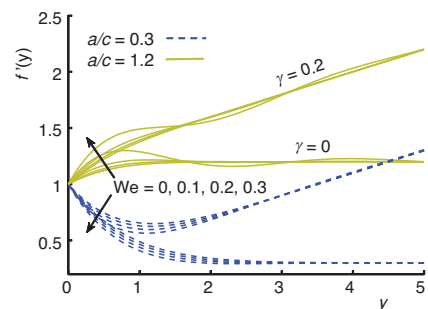


Figure 5. Velocity profile against y for the different values of We , a/c , and γ

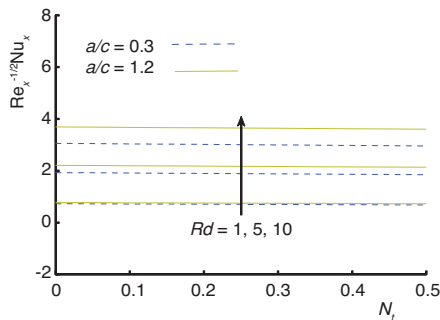


Figure 6. Variation of Nusselt number against N_t for the different values of Rd and a/c

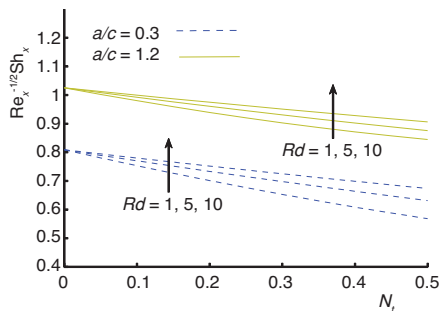


Figure 7. Variation of Sherwood number against N_t for the different values of Rd and a/c

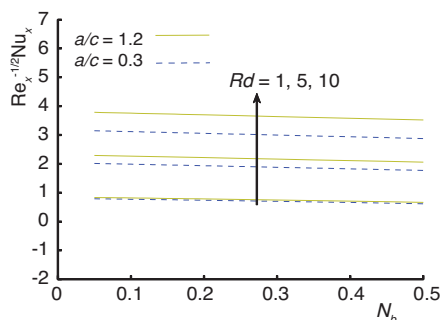


Figure 8. Variation of Nusselt number against N_b for the different values of Rd and a/c

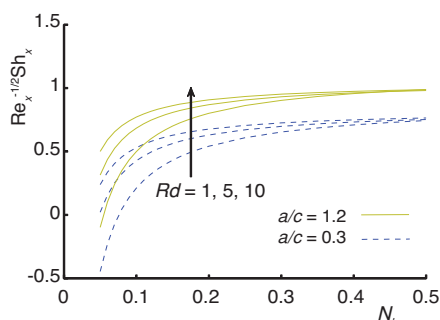


Figure 9. Variation of Sherwood number against N_b for the different values of Rd and a/c

Sherwood, $Re_x^{-1/2}Sh_x$, numbers are plotted against thermophoresis parameter, N_t , for the different values of Rd and a/c . It is clear from fig. 6 that with increase in the values of N_t , a very slight decrease in local Nusselt number is observed for both cases of a/c ($a/c > 1$, $a/c < 1$).

Consequently, temperature profile and thermal boundary layer thickness increase with increase of thermophoresis parameter, N_t , near the wall. Figure 7 elucidates that the local Sherwood number decreases with increase of N_t , as a consequence the concentration profile and concentration boundary layer increase with increase of N_t . From figs. 6 and 7, an increase in local Nusselt and local Sherwood numbers is observed due to enhancement of radiation. In figs. 8 and 9, the values of local Nusselt, $Re_x^{-1/2}Nu_x$, and local Sherwood, $Re_x^{-1/2}Sh_x$, numbers are plotted against Brownian motion parameter, N_b , for the different values of Rd and a/c . It is seen that with increase in Brownian motion the local Nusselt number decreases but the local Sherwood number increases.

This increase in local Sherwood number is very rapid in the range $0 < N_b < 0.2$. This phenomenon leads to increase the temperature and thermal boundary layer thickness but decrease in concentration profile.

In figs. 10 and 11, the variation of local Nusselt ($Re_x^{-1/2}Nu_x$) and local Sherwood ($Re_x^{-1/2}Sh_x$) numbers are plotted against Biot number (depending on the heat transfer coefficient) for the different values of Rd and a/c . It is seen that the local Nusselt number increases and local Sherwood number decreases for initial values of Biot number and for the larger values of Biot number both quantities become constant. Due to the larger values of $Bi \rightarrow \infty$ the surface become heated and heat transfer rate increases.

In fact, the larger values of Biot number imply the strong surface convection result in high surface temperature. Therefore, increase in Biot number enhanced the temperature and thermal boundary-layer thickness.

This behavior can be predicted from fig. 12. In fig. 13, concentration profile is plotted against y for different values of Biot number when $Rd = 2$ and $a/c = 0.3$. Concentration profile increases with increase in the values of Biot number because concentration distribution depends upon the temperature field hence the larger Biot number helps to increase the concentration of nanoparticles in fluid.

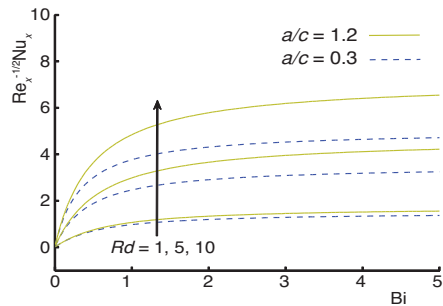


Figure 10. Variation of Nusselt number against Bi for the different values of Rd and a/c

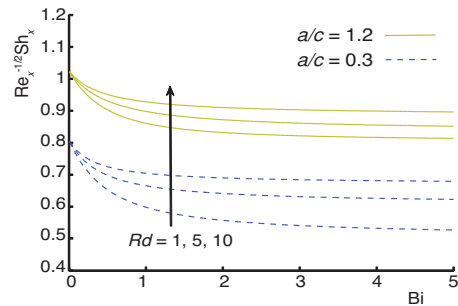


Figure 11. Variation of Sherwood number against Bi for the different values of Rd and a/c

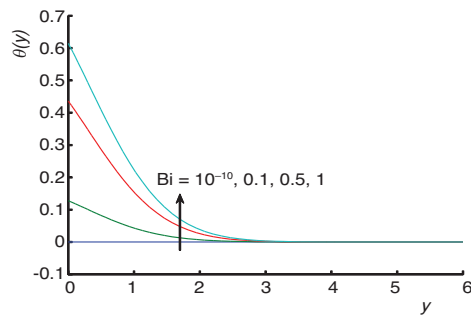


Figure 12. Temperature profile against y for the different values of Bi

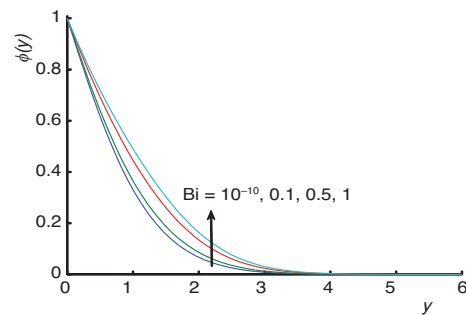


Figure 13. Concentration profile against y for the different values of Bi

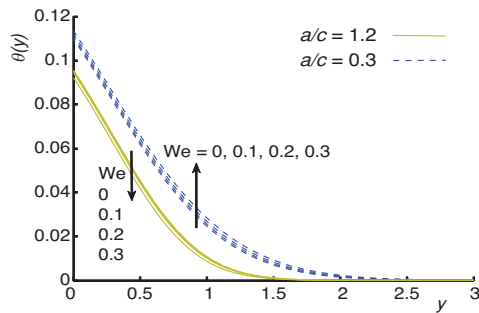


Figure 14. Temperature profile against y for the different values of We and a/c

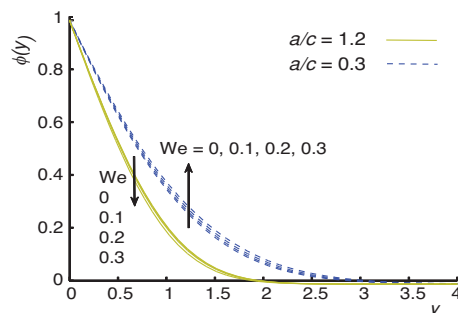


Figure 15. Concentration profile against y for the different values of We and a/c

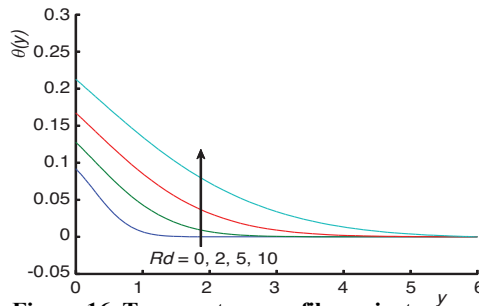


Figure 16. Temperature profile against y for the different values of Rd

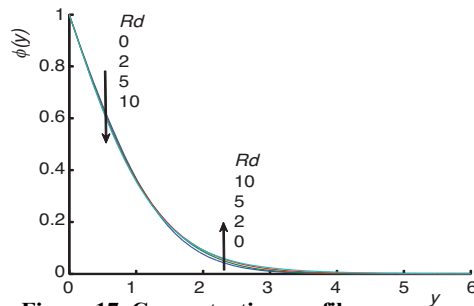


Figure 17. Concentration profile against y for the different values of Rd

In figs. 14 and 15 temperature and concentration profiles are plotted against y for the different values of Weissenberg number and a/c when $Rd = 1$, $Bi = 0.1$. For $a/c < 1$, it is observed that the temperature and concentration profiles are increasing functions of Weissenberg number but for $a/c > 1$ an opposite behavior is noted.

In figs. 16 and 17, temperature and concentration profiles are plotted against y for the different values of Rd when $Bi = 0.1$ and $a/c = 0.3$.

With increase in the values of radiation parameter, temperature of the fluid increases where the concentration profile decreases near the wall but for the larger value of y , it increases with increase in the values of radiation parameter.

Conclusions

The combined effect of radiation and convective boundary condition in the region of oblique stagnation point flow of elastico-viscous fluid saturated with nanoparticles is considered. The governing partial differential equations are transformed into system of ordinary differential equations by using the similarity transformation. The obtained system of equations is solved numerically by using CSNIS. The present numerical results are in excellent agreement with the previously obtained results. It is observed that the similarity eqs. (25)-(28) subject to the boundary conditions (29) have unique solution, dual solution and no solution in different region of the parameter Weissenberg number. For $a/c > 1$, the range of existence of solution increases due to increase in a/c and for $a/c < 1$, the range of unstable solution become larger than that of the stable solution. It is also concluded that.

- The velocity of the fluid intensifies due to increase in Weissenberg number when $a/c > 1$ but an opposite behavior is observed for $a/c < 1$.
- The velocity of the fluid is found an increasing function of γ .
- Temperature profile and thermal boundary layer thickness enhance due to increase in the values thermophoresis parameter.
- Concentration profile and concentration boundary layer thickness increase with increase of thermophoresis parameter.
- Brownian motion enhanced the thermal boundary layer thickness.
- Brownian motion decreases the concentration boundary layer thickness.
- The larger values of Biot number imply the enhancement in heat transfer and thermal boundary layer thickness.
- Concentration profile increases with increase in the values of Biot number.
- Temperature is noted an increasing function of radiation.

Acknowledgment

The authors are grateful to the editor and anonymous reviewers for their valuable suggestions that helped to improve the manuscript. The first author is thankful to HEC for financial assistance.

Nomenclature

a, b, c – positive constants

Bi – Biot number

C – solutal concentration

C_f – skin friction coefficient

C_p – specific heat constant

C_w – solutal concentration at the wall

C_∞ – ambient solutal concentration

D_B – Brownian diffusion coefficient

D_T – thermophoretic diffusion coefficient

f – dimensionless stream function

h_f – convective heat transfer coefficient

k – thermal conductivity of the nanofluid

k_ϕ – elasticity of fluid

N_b – Brownian motion parameter

N_t – thermophoresis parameter

Nu – Nusselt number

Pr	– Prandtl number	We	– Weissenberg number
p	– pressure of the fluid [Nm^{-1}]	x, y	– co-ordinates along and normal to the plate
q_m	– mass flux at the wall	<i>Greek symbols</i>	
q_r	– radiative heat flux	α_r	– Rosseland mean absorption
q_w	– heat flux at the wall	μ	– dynamic viscosity. [$\text{kgm}^{-1}\text{s}^{-1}$]
Re_x	– local Reynolds number	θ	– dimensionless temperature
Rd	– radiation conduction parameter or Planck number	ρ	– fluid density
Sc	– Schmidt number	$(\rho C)_f$	– heat capacity of the fluid
Sh_x	– local nanoparticle Sherwood number	$(\rho C)_p$	– effective heat capacity of the nanoparticle material
T	– temperature of the fluid in the boundary-layer	σ	– Stephen-Boltzmann constant
T_f	– temperature of the hot fluid	σ_s	– scattering coefficient
T_∞	– ambient fluid temperature	τ	– ratio between the effective heat capacity of the nanoparticle material and heat capacity of the fluid dynamic viscosity
T_w	– surface temperature	ν	– kinematic viscosity
U_e	– free stream velocity	Ψ	– stream function
u, v	– dimensionless velocity components in x- and y- directions		

References

- [1] Stuart, J. T., The Viscous Flow Near a Stagnation Point when the External Flow has Uniform Vorticity, *J. Aerospace Sci.*, 26 (1959), 2, pp. 124-125
- [2] Tamada, K. J., Two-Dimensional Stagnation-Point Flow Impinging Obliquely on an Oscillating Flat Plate, *J. Physical Soc. Jpn.*, 46 (1979), 1, pp. 310-311
- [3] Dorrepaal, J. M., An Exact Solution of the Navier-Stokes Equation which Describes Non-Orthogonal Stagnation-Point Flow in Two Dimension, *J. Fluid Mech.*, 163 (1986), Feb., pp. 141-147
- [4] Reza, M., Gupta, A. S., Steady Two-Dimensional Oblique Stagnation Point Flow towards a Stretching Surface, *Fluid Dynamic Research*, 37 (2005), 5, pp. 334-340
- [5] Chiam, T. C., Stagnation Point Flow Towards a Stretching Plate, *J. Phys. Soc. Jpn.*, 63 (1994), 6, pp. 2443-2444
- [6] Lok, Y. Y., et al., Non-Orthogonal Stagnation Point Flow towards a Stretching Sheet, *Int. J. Nonlin. Mech.*, 41 (2006), 4, pp. 622-627
- [7] Reza, M., Gupta, A. S., Some Aspects of Non-Orthogonal Stagnation-Point Flow towards a Stretching Surface, *Engineering*, 2 (2010), 9, pp. 705-709
- [8] Drazin, P. G., Riley, N., *The Navier-Stokes Equations, a Classification of Flows and Exact Solutions*, London Mathematical Society, Lecture Notes Series, Cambridge University Press, Cambridge, UK, 2007
- [9] Tooke, R. M., Blyth, M. G., A Note on Oblique Stagnation-Point Flow, *Phys. Fluids*, 20 (2008), 3, pp. 1-3
- [10] Weidman, P. D., Putkaradze, V., Axisymmetric Stagnation Flow Obliquely Impinging on a Circular Cylinder, *Eur. J. Mech. B. Fluids*, 22 (2003), 2, pp. 123-131
- [11] Weidman, P. D., Putkaradze, V., Erratum to Axisymmetric Stagnation Flow Obliquely Impinging on a Circular Cylinder, *Eur. J. Mech. B. Fluids*, 24 (2004), 6, pp. 788-790
- [12] Erfani, E., et al., The Modified Differential Transform Method for Solving Off-Centered Stagnation Flow Toward a Rotating Disc, *Int J Comput Methods*, 7 (2010), 4, pp. 655-670
- [13] Husain, I., et al., Two-Dimensional Oblique Stagnation Point Flow towards a Stretching Surface in a Viscoelastic Fluid, *Central Eur. J. Phys.* 9 (2011), 1, pp. 176-182
- [14] Mahapatra, T. R., et al., Oblique Stagnation-Point Flow and Heat Transfer towards a Shrinking Sheet with Thermal Radiation, *Meccanica*, 47 (2012), 6, pp. 1325-1335
- [15] Lok, Y. Y., et al., Oblique Stagnation Slip Flow of a Micropolar Fluid, *Mechanica*, 45 (2010), 2, pp. 187-198
- [16] Yajun, L. V., Liancun, Z., MHD Oblique Stagnation-Point Flow and Heat Transfer of a Micro Polar Fluid towards to a Moving Plate with Radiation, *Int. J. Eng. Sci. Innovative Tech*, 2 (2013), 2, pp. 200-209
- [17] Javed, T., et al., Numerical Study of Unsteady Oblique Stagnation Point Flow Over a Oscillating Flat Plate, *Can J. Phys.*, 93 (2015), 10, pp. 1138-1143
- [18] Buongiorno, J., Hu, L. W., Nanofluid Coolants for Advanced Nuclear Power Plants, *Proceedings, ICAPP*, Seoul, 2005, Paper No. 5705, pp. 15-19
- [19] Maxwell, J. C., *A Treatise on Electricity and Magnetism*, 2nd ed., Oxford Univ. Press, Cambridge, UK, 1904

- [20] Choi, S. U. S., Enhancing Thermal Conductivity of Fluids with Nanoparticles, in: Developments and Application of Non-Newtonian Flows, *ASME , FED-Vol. 231/MD-Vol. 66* (1995), pp. 99-105
- [21] Buongiorno, J., Convective Transport in Nanofluids, *ASME J. Heat Transfer*, 128 (2006), 3, pp. 240-250
- [22] Kuznetsov, A. V., Nield, D. A., Natural Convective Boundary-Layer Flow of a Nanofluid Past a Vertical Plate, *Int. J. Thermal Sci.*, 49 (2010), 2, pp. 243-247
- [23] Kuznetsov, A. V., Nield, D. A., Double-Diffusive Natural Convective Boundary-Layer Flow of a Nanofluid Past a Vertical Plate, *Int J Thermal Sci*, 50 (2011), 5, pp. 712-717
- [24] Makinde, O. D., Aziz, A., Boundary Layer Flow of a Nanofluid Past a Stretching Sheet with a Convective Boundary Condition, *Int. J. Thermal Sci.*, 50 (2011), 7, pp. 1326-1332
- [25] Hassani, M., et al., An Analytical Solution for Boundary Layer Flow of a Nanofluid Past a Stretching Sheet, *Int. J. Therm. Sci.*, 50 (2011), 11, pp. 2256-2263
- [26] Rana, P., Bhargava, R., Flow and Heat Transfer of a Nanofluid over a Nonlinearly Stretching Sheet: A Numerical Study, *Commun Nonlinear Sci. Numer Simulat*, 17 (2012), 1, pp. 212-226
- [27] Hamad, M. A. A., Ferdows, M., Similarity Solution of Boundary Layer Stagnation-Point Flow towards a Heated Porous Stretching Sheet Saturated with a Nanofluid with Heat Absorption/Generation and Suction/Blowing: A Lie Group Analysis, *Commun Nonlinear Sci Numer Simulat*, 17 (2012), 1, pp. 132-40
- [28] Sheikholeslami, M., et al., Numerical Simulation of Two Phase Unsteady Nanofluid Flow and Heat Transfer Between Parallel Plates in Presence of Time Dependent Magnetic Field, *J. Taiwan Institute Chem. Eng.*, 46 (2015), Jan., pp. 43-50
- [29] Turkyilmazoglu, M., Nanofluid Flow and Heat Transfer due to A Rotating Disk, *Computer and Fluids*, 94 (2014), May, pp. 139-146
- [30] Rahman, M. M., et al., Boundary Layer Flow of a Nanofluid Past a Permeable Exponentially Shrinking/Stretching Surface with Second Order Slip Using Buongiorno's Model, *Int. J. Heat Mass Transfer*, 77 (2014), Oct., pp. 1133-1143
- [31] Rashidi, M. M., et al., Buoyancy Effect on MHD Flow of Nanofluid over a Stretching Sheet in the Presence of Thermal Radiation, *J. Molecular Liquids*, 198 (2014), Oct., pp. 234-238
- [32] Kameswaran, P. K., et al., Homogeneous-Heterogeneous Reactions in a Nanofluid Flow Due to a Porous Stretching Sheet, *Int. J. Heat Mass Transfer*, 57 (2013), 2, pp. 465-472
- [33] Abbasi, F. M., et al., Peristaltic Transport of Magneto-Nanoparticles Submerged in Water: Model For Drug Delivery System, *Phasica E*, 68 (2015), Apr., pp. 123-132
- [34] Bachok, N., et al., Boundary-Layer Flow of Nanofluids over a Moving Surface in a Flowing Fluid, *Int. J. Thermal Sci.*, 49 (2010), 9, pp. 1663-1668
- [35] Sebdani, S. M., et al., Effect of Nanofluid Variable Properties on Mixed Convection in a Square Cavity, *Int. J. Thermal Sci.*, 52 (2012), Feb., pp. 112-126
- [36] Rashidi, M. M., et al., Lie Group Solution for Free Convective Flow of a Nanofluid Past a Chemically Reacting Horizontal Plate in a Porous Media, *Math Probl Eng.*, 2014 (2014), ID 239082
- [37] Abolbashari, M. H., et al., Entropy Analysis for an Unsteady MHD Flow Past a Stretching Permeable Surface in Nanofluid, *Powder Technol.*, 267 (2014), Nov., pp. 256-267
- [38] Makinde, O. D. Analysis of Sakiadis Flow of Nanofluids with Viscous Dissipation and Newtonian Heating, *Appl Math Mech.*, 33 (2012), 12, pp. 1545-1554
- [39] Hayat, T., et al., Heat Transfer Analysis in the Flow of Walters' B Fluid with a Convective Boundary Condition, *Chin. Phys. B*, 23 (2014), 8, 084701
- [40] Husain, I., et al., Two-Dimensional Oblique Stagnation-Point Flow towards a Stretching Surface in a Viscoelastic Fluid, *Cent. Eur. J. Phys.*, 9 (2011), 1, pp. 176-182
- [41] Beard, D. W., Walters, K., Elastico-Viscous Boundary-Layer Flows. I: Two-Dimensional Flow Near a Stagnation Point, *Proc. Cambridge Philos. Soc.*, 60 (1964), 3, pp. 667-674
- [42] Garg, V. K., Rajagopal, K.R., Flow of a Non-Newtonian Fluid Past a Wedge, *Acta Mech.*, 88 (1991), 1-2, pp. 113-123
- [43] Vajravelu K., Roper T., Flow and Heat Transfer in a Second Grade Fluid over a Stretching Sheet, *Int. J. Non-linear Mech.*, 34 (1999), 6, pp. 1031-1036
- [44] Motsa, S. S., et al., Spectral Relaxation Method and Spectral Quasi-Linearization Method for Solving Unsteady Boundary Layer Flow Problems, *Advances in Mathematical Physics*, 2014 (2014), ID 341964
- [45] Motsa, S. S., A New Spectral Local Linearization Method for Nonlinear Boundary Layer Flow Problems, *Journal of Applied Mathematics*, 2013 (2013), Article ID 423628
- [46] Trefethen, L. N., *Spectral Methods in MATLAB*, Society for Industrial and Applied Mathematics, SIAM, Philadelphia, Penn., USA, 2000

- [47] Labropulu, F., *et al.*, Non-Orthogonal Stagnation-Point Flow towards a Stretching Surface in a Non-Newtonian Fluid with Heat Transfer, *Int. J. Therm. Sci.*, 49 (2010), 6, pp. 1042-1050
- [48] Weidman, P. D., *et al.*, The Effect of Transpiration on Self-Similar Boundary Layer Flow over Moving Surfaces, *Int. J. Eng. Sci.*, 44 (2006), 11-12, pp. 730-737
- [49] Paullet, J., Weidman, P., Analysis of Stagnation Point Flow toward a Stretching Sheet, *Int. J. Nonlinear Mech.*, 42, (2007), 9, pp. 1084-1091
- [50] Rosca, A. V., Pop, I., Flow and Heat Transfer over a Vertical Permeable Stretching/ Shrinking Sheet with a Second Order Slip, *Int. J. Heat Mass Transfer*, 60 (2013), May, pp. 355-364